A SAR-based Measurement Method for Passive-Tag Positioning with a Flying UHF-RFID Reader

A. Buffi, *Member*, *IEEE*, A. Motroni, *Student Member*, *IEEE*, P. Nepa, *Member*, *IEEE*, B. Tellini, *Member*, *IEEE,* and R. Cioni

***Abstract*—This paper presents and characterizes a measurement method for positioning of passive tags, by a drone equipped with a UHF-RFID reader. The method is based on a Synthetic Aperture Radar (SAR) approach and exploits the knowledge of the reader/drone trajectory, which is achieved with a differential Global Navigation Satellite System. Different sources of measurement uncertainty are analysed by means of numerical simulations and experimental results. The method capabilities are discussed versus the length and shape of the reader trajectory. Finally, the proposed localization method is validated through an experimental analysis carried out with commercial RFID hardware and a micro-class unmanned aerial vehicle.**

***Index Terms*— UHF-RFID Measurement Method; UHF-RFID Position Measurement; UHF-RFID Localization; RFID drone; RFID UAV; Flying reader; Tag localization; Tag positioning.**

I. Introduction

In the last years, drones received great attention for their capability to reach places that are dangerous or not easily accessible to humans, or to monitor huge spaces as an effective alternative to wide sensor networks [1]. They are employed for aerial photogrammetry [2], gas detection [3], precision agriculture, structural monitoring and so on [4]-[5]. More recently, drones equipped with barcode readers were employed for item management in indoor warehouses [6] and for home delivery [7].

In many scenarios, the RFID technology could expand the drone activities by implementing simultaneous identification [8]-[9] and localization [10]-[11] features. A drone equipped with a RFID reader can locate tagged items within an indoor or outdoor scenario; alternatively, a set of grounded RFID antennas can localize a drone equipped with a passive tag [12].

As in wireless sensor networks, some systems based on Received Signal Strength Indicator (RSSI) [13]-[14] were recently proposed to measure the drone location [15] or the tag location [16]-[17]. The work in [15] proposes a device-free UHF-RFID localization scheme to locate an Unmanned Aerial Vehicle (UAV). The method exploits the RSSI changes induced by the presence of metallic objects. Thus, the stationary reader detects the tag RSSIs during the drone flight and determines the group of tags affected by larger variations. From the latter information the UAV position is estimated. In [16], a localization system performs environmental monitoring through an UAV equipped with a 433 MHz RFID reader. After tag detection, the UAV continues to rotate in the area performing RSSI measurements and then estimates the tag distance through an assumed path loss model. Then, by knowledge of the drone position through the Global Navigation Satellite System (GNSS) receiver, a multilateration algorithm provides the position of the static detected tag.

As known in the literature, solutions based on the phase of the tag-backscattered signal [18] are more accurate than RSSI-based techniques. Multiple antenna solutions employ two [19] or more antennas [20] to measure the Angle of Arrival (AoA). Alternatively, synthetic array methods exploit the relative motion between a single reader antenna and the tags [21]. The latter can find application to locate moving tags with respect to a fixed reader antenna, by resembling an Inverse Synthetic Aperture Radar (ISAR) approach [22]-[23], as well as to locate fixed tags, through a moving reader antenna and a Synthetic Aperture Radar (SAR) approach [24]-[25].

The authors of this paper recently proposed the employment of the SAR-based localization method [21] to measure the position of fixed RFID tags, by a drone equipped with a UHF-RFID reader [10]. The 1D localization capability was originally shown in [10] through a phase-based processing, together with preliminary results on the 2D localization. In such framework, it is noteworthy

Manuscript received April 5, 2018, Accepted July 1, 2018.

A. Buffi (corresponding author: phone: +39-050-2217379) and B. Tellini are with the Department of Energy, Systems, Territory and Constructions Engineering, University of Pisa, Pisa, Italy (e-mail: alice.buffi@unipi.it, bernardo.tellini@unipi.it).

A. Motroni and P. Nepa are with the Department of Information Engineering, University of Pisa, Pisa, Italy (e-mail: andrea.motroni@ing.unipi.it, paolo.nepa@unipi.it).

R. Cioni is with IDS, Ingegneria dei Sistemi, Pisa (e-mail: r.cioni@idscorporation.com).

the solution proposed in [26], where a drone equipped with two antennas works as a relay of the RFID signal to reduce the payload and increase the reading range. The two antennas permit a full-duplex wireless communication between a UHF-RFID reader placed on the ground and tags deployed in the environment. Since the mobile relay preserves phase and timing characteristics of the forwarded signal, a phase-based tag localization can be performed.

This paper describes the SAR-based method [21] employing both amplitude and phase of the tag backscattered signal for measuring the tag 2D position. Section II illustrates the signal model and the localization algorithm. Section III presents the method characterization through an analysis of the possible sources of uncertainty. Then, Section IV describes the experimental setup with commercial RFID hardware and a micro-class unmanned aerial vehicle, while Section V depicts the results of the experimental analysis in a real outdoor scenario. Finally, some conclusions are drawn in Section VI.

II. The SAR-based Methodology

Fig. 1 depicts an outdoor warehouse, a drone equipped with a RFID reader and several items tagged with passive transponders (tags). As the signal backscattered by the passive tag contains the tag unique identifier (Electronic Product Code, EPC), the system in Fig. 1 may implement an efficient real-time inventory technique.

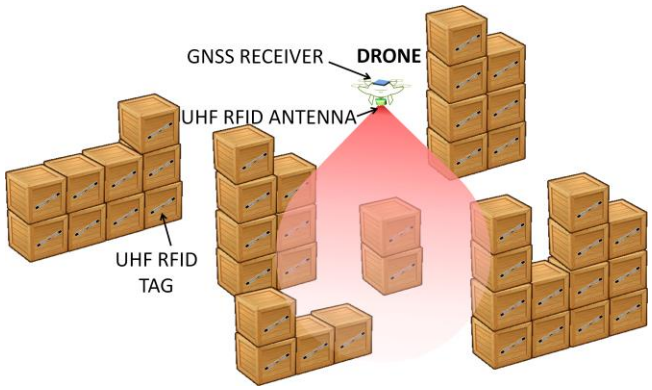

Fig. 1. Sketch of tagged items in an outdoor warehouse, where a drone equipped with a GNSS receiver and a UHF-RFID reader can identify and localize all the detected tags.

The passive RFID technology at the UHF band guarantees a reading range of several meters, so being a valuable solution in the considered scenario with respect to RFID technologies at lower frequencies that exhibit lower reading ranges and read rates. The detection range of the UHF-RFID system mainly depends on the tag chip sensitivity, as the transmitted power and the antenna gain at the reader side are limited by international regulations, and last-generation chips can guarantee reading ranges larger than 10 m. Moreover, a wide-beam reader antenna allows detecting many tags, which can be managed simultaneously thanks to the anti-collision algorithm implemented in the EPC Global Class1 Gen2 protocol [27]. By exploiting the movement of the flying reader antenna with respect to the static tags, the adverse effects of the shadowing and multipath phenomena are severely attenuated, and a high inventory performance may be achieved.

Additionally, the SAR-based method proposed by the authors in [21]-[22] can be implemented to measure the position of every detected tag by exploiting the knowledge of the instantaneous reader antenna position during the flight, which can be measured through a GNSS receiver on the drone, in an outdoor scenario.

A. *Signal model*

When the reader antenna carried by the drone flies over a tag, the backscattered complex signal (named as complex signal hereafter) depends on the relative distance r_n between the reader antenna and the tag position $\mathbf{p_{tag}} = \left[x_{tag}, y_{tag}, z_{tag} \right]$ as:

$$s_n\left(\mathbf{p_{tag}}\right) = A_n e^{-j\phi_n} = A_n e^{-j\left(\phi_0 + 4\pi r_n/\lambda\right)}, \quad n = 1, \ldots, N_r \qquad (1)$$

where A_n is the amplitude of the tag complex signal, λ is the free-space wavelength of the radiated field, N_r is the number of available successful readings while ϕ_0 is the phase offset including the effect of cables and other reader components [18]. In particular, in our model ϕ_0 is assumed constant. Thus, the variations of the complex signal during the drone flight are related to the variations of the distance r_n:

$$r_n = \left\| \mathbf{p_n} - \mathbf{p_{tag}} \right\| \quad n = 1, \ldots, N_r . \qquad (2)$$

In (2), $\|\,.\,\|$ is the norm operator of the distance vector between the unknown tag position $\mathbf{p_{tag}}$ and the instantaneous reader antenna position $\mathbf{p_n} = [x_n,\ y_n,\ z_n]$ along the drone path. The latter can be modelled as:

$$\mathbf{p_n} = \mathbf{p_{n\text{-}GNSS}} + \Delta\mathbf{p_{APC\text{-}GNSS}} \qquad (3)$$

where, $\mathbf{p_{n\text{-}GNSS}} = [x_{n-GNSS},\ y_{n-GNSS},\ z_{n-GNSS}]$ is the GNSS instantaneous antenna position and $\Delta\mathbf{p_{APC\text{-}GNSS}}$ is the relative position of the RFID antenna phase centre with respect to the GNSS antenna phase centre.
A_n can be described as [28]:

$$A_n = \frac{\sqrt{\Delta\sigma}}{2} f^2(\theta_n) \frac{1}{r_n^2} \qquad n = 1,\ \ldots,\ N_r, \qquad (4)$$

where $\Delta\sigma$ is the tag differential backscattered cross section [18], $f(\theta_n)$ is the radiation pattern of the reader antenna, θ_n indicates the tag angular position with respect to the reader antenna at the time of the *n*-reading, and $1/r_n^2$ is the two-way free-space propagation loss in line-of-sight condition.
In this work, the radiation pattern of the reader antenna $f(\theta_n)$ is modelled by considering a quadratic cosine function:

$$f(\theta_n) = \cos^2(\theta_n) \qquad n = 1,\ \ldots,\ N_r \qquad (5)$$

Thus, the corresponding half power beam width (HPBW) is equal to 65°, which is close to the typical value for commercial UHF-RFID reader antennas [29].

B. SAR-based localization algorithm

Let us consider the variations of the complex signal with respect to the value assumed at an assigned reference time, namely the *relative history* of the backscattered complex signal. Therefore, we can remove the constant ϕ_0. Let us assume the first available reading as our reference, thus from (1) we have:

$$\Delta s_n = \frac{s_n}{s_1} = \frac{A_n}{A_1} e^{-j(\phi_n - \phi_1)} \qquad n = 1,\ \ldots,\ N_r \qquad (6)$$

The resulting normalized phasor sequence can be written as:

$$\mathbf{y_{AP}}(\mathbf{p_{tag}}) = \left[1,\ \Delta s_2,\ \ldots,\ \Delta s_{N_r}\right]^T \qquad (7)$$

being '*T*' the transpose operator. For a given path of the reader antenna, $\mathbf{y_{AP}}$ varies as a function of the actual tag position.
For a defined drone trajectory, a set of nominal normalized phasor sequences can be computed analytically, for hypothesized values $\mathbf{p_{tag}}' = [x_{tag}',\ y_{tag}',\ z_{tag}']$ of the tag spatial coordinate $\mathbf{p_{tag}}$, according to the (7):

$$\mathbf{a}(\mathbf{p_{tag}}') = \left[1,\ \Delta s_2',\ \ldots,\ \Delta s_{N_r}'\right]^T \qquad (8)$$

where $\Delta s_n' = s_n'/s_1'$ and $s_n' = s_n(\mathbf{p_{tag}}')$ according to (1).
The best match between (7) and (8) can be found through the normalized spatial-domain cross-correlation (matching function):

$$\mathbf{C_{AP}} = \frac{\left|\mathbf{a}^{\mathbf{H}}(\mathbf{p_{tag}}')\mathbf{y_{AP}}\right|^2}{\left\|\mathbf{a}^{\mathbf{H}}(\mathbf{p_{tag}}')\right\|^2 \cdot \left\|\mathbf{y_{AP}}\right\|^2}, \qquad (9)$$

with 'H' the Hermitian (conjugate transpose) operator. The cross correlation in (9) is calculated over the grid of $\mathbf{p_{tag}}'$ values for which the nominal normalized phasor sequences were computed. The peak position of (9) provides an estimate of the tag spatial coordinates $\mathbf{p_{tag}} = \left[x_{tag},\ y_{tag},\ z_{tag} \right]$:

$$\mathbf{p_{tag}} = \arg\max_{\mathbf{p_{tag}}'} \mathbf{C_{AP}} \qquad (10)$$

Higher the peak value C_{peak}, greater the similarity between the tag complex signal and the nominal one.

The limit for the spatial sampling is chosen according to the sampling theorem [30] and in our case reads as [22]:

$$\left\| \mathbf{p_{n+1}} - \mathbf{p_n} \right\| \le \lambda / \left[4 \sin\left(HPBW/2 \right) \right] \qquad (11)$$

Due to the anti-collision protocol [31], a random time slot is associated to each tag to backscatter its own EPC during the reader inventory. Consequently, readings are collected with a non-uniform sampling. However, if consecutive readings satisfy (11), the complex signal can be successfully recognized and the method here proposed can estimate the tag position without ambiguity.

In the considered scenario, tags are at ground level, thus their z-coordinate (z_{tag}) is assumed as a zero reference level and the SAR-based localization algorithm is used to estimate the tag 2D coordinates $\mathbf{p_{tag}} = \left[x_{tag},\ y_{tag},\ 0 \right]$.

For the more general case of an arbitrary z-coordinate (fully 3D localization), the proposed localization method can still be applied by varying the hypothesized values of the three coordinates $\left(x_{tag}',\ y_{tag}',\ z_{tag}' \right)$, instead of only two $\left(x_{tag}',\ y_{tag}' \right)$, but then a quite larger computational time must be tolerated. On the other hand, the computational time can be reduced to acceptable values if the localization procedure (9) is performed through space-efficient search algorithms.

III. Characterization of the Measurement Method

In SAR-based localization methods, the difference between the peak position $\mathbf{p_{tag}}$ (estimated tag position) and the actual tag position $\mathbf{p_{tag}}$ represents the measurement error, which is investigated separately for the x- and y- coordinates: $\varepsilon_x = x_{tag} - x_{tag}$ and $\varepsilon_y = y_{tag} - y_{tag}$.

By analysing the shape of the 2D matching function, it is also possible to characterize the associated uncertainty. In particular, narrower the mainlobe and lower the secondary lobes, smaller is the uncertainty. Thus, the main axes of the -3 dB mainlobe ($W_{maj} \times W_{min}$) were considered through the paper as the dispersion index of the estimated tag position, together with the -3 dB widths along x- (W_x) and y- (W_y) directions. Besides, the level of the secondary lobes with respect to the matching function peak, which is named as peak-to-sidelobe ratio (*PSLR*) [32] within SAR nomenclature, was investigated.

As an example, the 2D matching function for the case of an L-shape trajectory of the reader antenna is represented in Fig. 2a with respect to the xy plane of the hypothetical tag coordinates $\mathbf{p_{tag}}' = \left[x_{tag}',\ y_{tag}' \right]$ (circle markers denote the assumed drone trajectory). The L-shape trajectory goes from point A [-1, 1, 3] m to point B [1, -1, 3] m, holding always the same height from the ground level, z_n=3 m.

For all simulated results in this section, the operating frequency is f_0=867.5 MHz (ETSI channel 13), corresponding to a wavelength of $\lambda = 34.6\,\text{cm}$. The actual tag position is $\left[x_{tag},\ y_{tag},\ z_{tag} \right] = [-1,\ -1,\ 0]\ \text{m}$ and its differential backscattered cross section was supposed constant along the path.

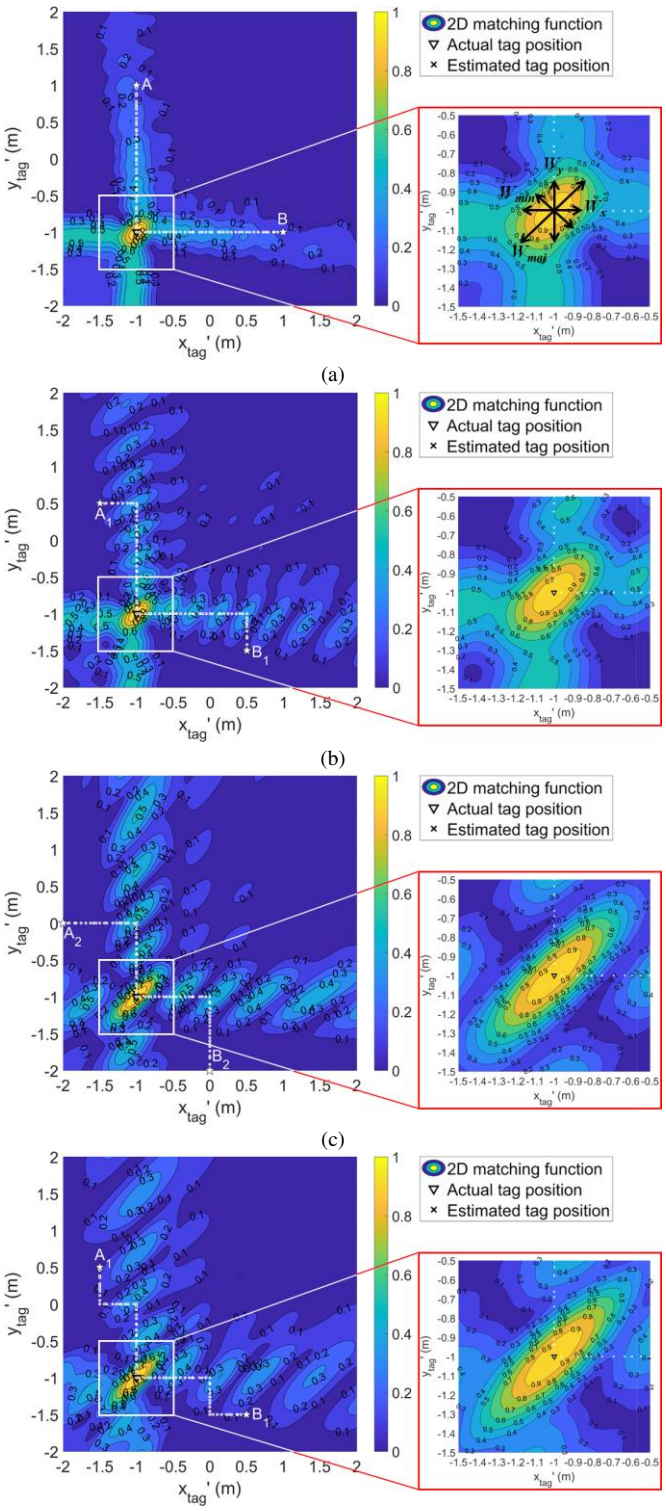

Fig. 2. Simulated matching function with respect to the hypothetical tag coordinates in the *xy*-plane, when considering different trajectories of the reader antenna. The actual tag position is $[x_{tag}, y_{tag}, z_{tag}]$=[-1, -1, 0] m and other system parameters are: f_0=867.5 MHz, N_r=81, D_x=D_y=2 m. (a) L-shape. (b) L_1-shape trajectory. (c) L_2-shape trajectory. (d) L_3-shape trajectory.

The synthetic aperture lengths along the *x*- (D_x) and *y*- (D_y) directions are equal to 2 m. N_r=81 consecutive readings were collecting considering an antenna beamwidth *HPBW*=65°. To emulate the non-uniform sampling given by the anticollision protocol, the drone position along the trajectory, for each one of the above readings, was derived by considering consecutive spatial steps whose width is a random variable with a uniform distribution in the [1, 9] cm interval.

Without any other source of error apart from numerical approximation, a practically vanishing localization error can be observed. The -3 dB mainlobe sizes are $W_{maj} \times W_{min}$=45 cm × 26 cm, while the mainlobe sizes along the *x*- and *y*- directions are W_x=W_y=31 cm. The sidelobe (*SL*) is equal to 0.59 with a consequent *PSLR*=1.71.

A. *Analysis of trajectories*

A series of numerical simulations were carried out to characterize the effect of the reader antenna trajectory on the lobe shape of the matching function. The 2D matching functions for other three reader antenna paths are represented in Fig. 2. As for the L-shape trajectory of Fig. 2a, the whole synthetic aperture lengths are equal to D_x=D_y=2 m, thus they differ only for the path shape. For the L_1-shape trajectory (Fig. 2b), the reader antenna moves from point A_1 [-1.5, 0.5, 3] m to point B_1 [0.5, -1.5, 3] m with a folded L-shape path. For the L_2-shape trajectory (Fig. 2c), the reader antenna moves from point A_2 [-2, 0, 3] m to point B_2 [0, -2, 3] m with a turned double L-shape path. For the L_3-shape trajectory (Fig. 2d), the reader antenna moves still from point A_1 to point B_1 but with a triple L-shape path. For all of them, the reader antenna height was constant at z_n=3 m from the ground level along the path; the actual tag position is still at $\left[x_{tag}, y_{tag}, z_{tag}\right] = [-1,\ -1,\ 0]$ m and N_r=81 tag readings were collected along the trajectory.

The phase of the normalized phasor sequence (6) for the considered trajectories is represented in Fig. 3a, while Fig. 3b depicts the amplitude of the normalized phasor sequence. The -3 dB mainlobe sizes and peak-to-sidelobe ratio are summarized in Table I. In particular, the L_1-shape trajectory is associated with a smaller mainlobe size, while the *PSLR* is higher for the L_3-shape trajectory. This confirms that the matching function is strictly dependent on the reader antenna trajectory with respect to the tag location.

During the drone flight, some spatial fluctuations can occur and the its path will never be exactly straight. An example of a perturbed L-shape trajectory from point A to point B is represented in Fig. 4 (N_r=405). The maximum excursions along the *x*- and *y*-directions are $\Delta_x = \Delta_y = 20$ cm. As apparent, the proposed SAR-based method is still able to measure the tag position with a satisfactory accuracy. Moreover, such fluctuations with respect to the rectilinear trajectory determine roughly the same mainlobe of the 2D matching function of Fig. 2a ($W_{maj} \times W_{min}$=45 cm × 25 cm, W_x=29 cm and W_y=30 cm), but the level of the side lobe decreases (*SL*=0.52) with a consequent improvement of the peak-to-sidelobe ratio (*PLSR*=1.91).

Some Montecarlo simulations (50 test cases) were carried out by considering different dynamics of the trajectory fluctuations. The mean value of -3 dB mainlobe sizes and of the *PLSR* are described in Table II, for different values of the fluctuation dynamics: $\Delta_x, \Delta_y \in [0.1,\ 0.2,\ 0.3,\ 0.4]$ m. The mainlobe sizes are nearby the same, while, the *PSLR* increases for higher dynamics. This latter result suggests that drone fluctuations can be profitably employed to reduce the contribution to the uncertainty for the tag position measurement.

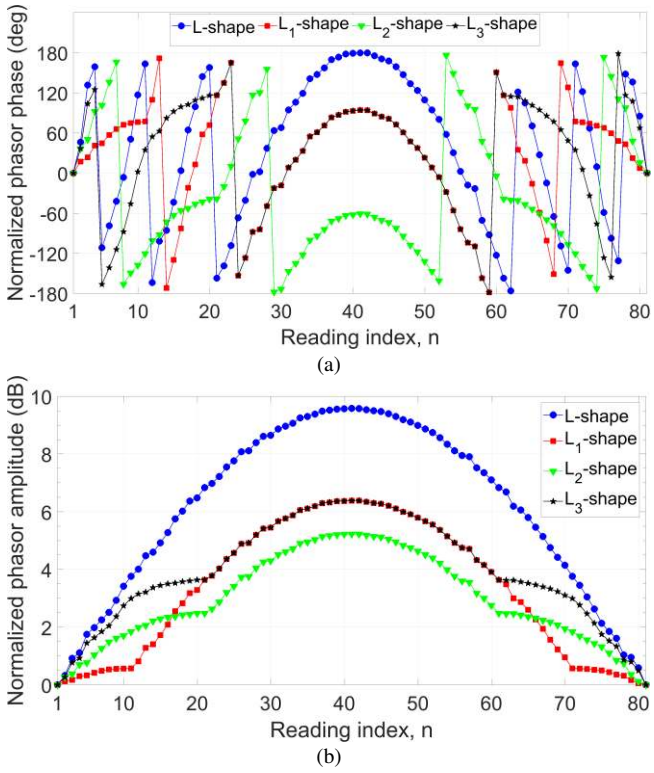

Fig. 3. (a) Relative phase and (b) relative amplitude of the simulated phasor sequence with respect to the reading index *n*, by considering different trajectory shapes as in Fig. 2.

TABLE I

MAINLOBE SIZES AND *PSLR* OF THE 2D MATCHING FUNCTION OBTAINED BY APPLYING THE SAR-BASED METHOD FOR DIFFERENT TRAJECTORIES OF THE FLYING READER ANTENNA.

Trajectory	L-shape	L_1-shape	L_2-shape	L_3-shape
W_{maj} (cm)	45	49	70	73
W_{min} (cm)	26	24	21	21
W_x (cm)	31	29	27	28
W_y (cm)	31	29	27	28
PSLR	1.71	1.73	1.88	2.06

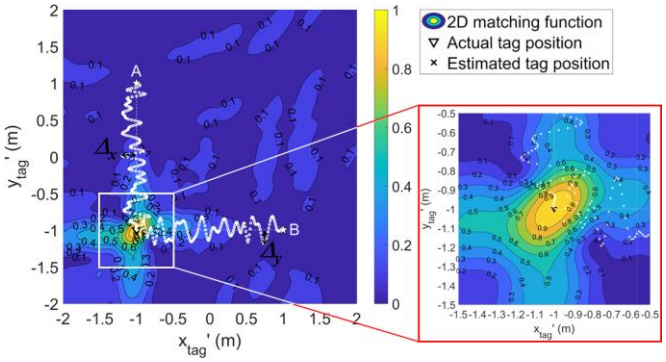

Fig. 4. Simulated matching function with respect to the hypothetical tag coordinates in the *xy* plane, when considering an L-shape trajectory of the reader antenna with fluctuation dynamics Δ_x=Δ_y=20 cm. The actual tag position is [x_{tag}, y_{tag}, z_{tag}]=[-1, -1, 0] m. Other system parameters are as in Fig. 2.

TABLE II

MAINLOBE SIZE AND *PSLR* OF THE 2D MATCHING FUNCTION OBTAINED BY VARYING THE FLUCTUATION DYNAMICS. AN L-SHAPE TRAJECTORY OF THE READER ANTENNA WAS CONSIDERED.

Δ (cm)	10	20	30	40
W_{maj} (cm)	46	45	44	42
W_{min} (cm)	25	25	25	24
W_x (cm)	31	30	30	29
W_y (cm)	31	30	30	29
PSLR	1.77	1.90	2.95	4.24

B. Antenna trajectory and RFID measurement uncertainty evaluation

To evaluate the uncertainty contribution associated with the reader antenna trajectory and the RFID measurements, we carried out a Montecarlo analysis performing 1000 test cases for the L-shape trajectory (Fig. 2a) of the flying reader antenna (D_x=D_y=2 m).

We assumed a uniformly distributed error in the interval between -2 cm and 2 cm for the GNSS receiver antenna position. Then, according to the Impinj datasheet [33], the standard deviation of RSSI and phase measurements were chosen equal to $\sigma_{RSSI} = 1$ dBm and $\sigma_\phi = 0.1$ rad, respectively. We recall that the RSSI parameter is a power level measurement [34]-[35]. Thus, the backscattered signal amplitude A_n, is evaluated from RSSI parameter in dBm as: $A_n = \sqrt{10^{RSSI_n\,[dBm]/10}}$.

The histogram of the measurement errors ε_x (blue bar) and ε_y (red bar) are represented Fig. 5. Errors are of centimetre order, with mean value and standard deviation equal to [μ_x, σ_x]=[0.9, 0.9] cm and [μ_y, σ_y]=[1.0, 0.9] cm for the *x*-coordinate and the *y*-coordinate, respectively. The maximum measurement error is 6 cm for both coordinates.

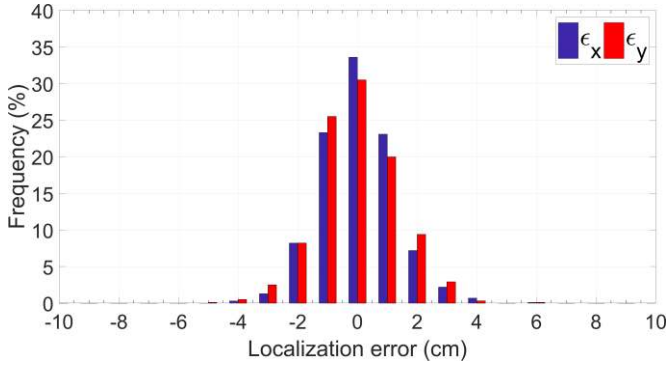

Fig. 5. Histogram of the measurement errors ε_x (blue bar) and ε_y (red bar), by considering the sources of error due to the GNSS receiver and the RFID measurements. 1000 Montecarlo simulations were performed by considering 10 tags. Other system parameters are as in Fig. 2.

IV. Experimental Setup

The experimental setup was realized by employing commercial RFID hardware and a micro-class unmanned aerial vehicle.

A. Hardware integration on drone

The commercial Colibrì IA-3 drone by IDS [36] was adopted for our measurements (Fig. 6). The drone has a diameter of 81 cm, a height of 28 cm, and a payload of 1 kg. It was equipped with a Compact Dual Frequency GNSS Board TOPCON B110 [37]. By means of a simultaneous acquisition with a Leica GS15 GPS/GLONASS fixed station (Fig. 7a), it is possible to adopt a post processing kinematics (PPK) methodology. This allows to estimate the drone position with an error lower than 2 cm, when the positioning rate is equal to 200 ms. The absolute position of the GNSS ground station was determined with the ITALPos network [38]. The GNSS data recorded on-board during the flight were processed using the PPK methodology to get the geographical coordinates of the drone trajectory.

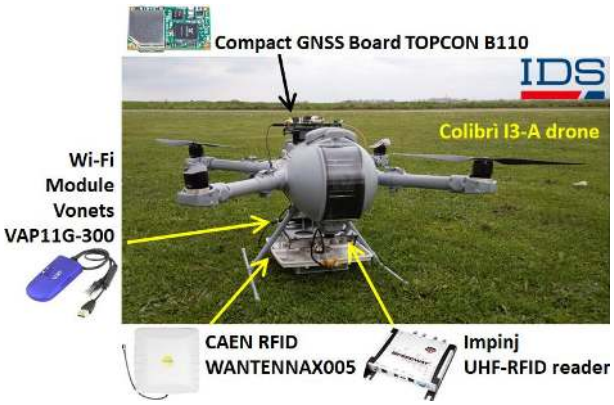

Fig. 6. Colibrì I3-A drone by IDS, equipped with GNSS module and UHF-RFID reader and antenna.

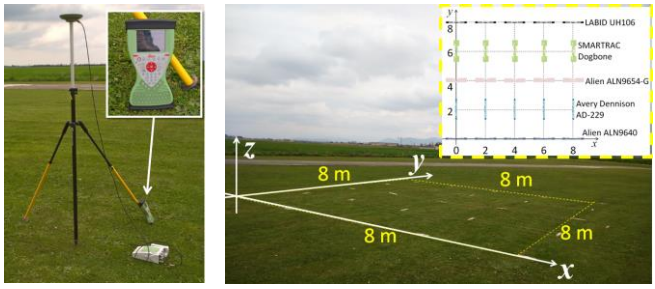

(a) (b)

Fig. 7. (a) Leica GS15 GPS/GLONASS fixed station employed for drone position measurements through the post processing kinematics methodology. (b) Measurement setup with a grid of 5 × 5 tags with inter-tag distance equal to 2 m, which are deployed in a 8 m × 8 m area.

The Impinj Speedway Revolution R420 UHF-RFID reader was installed on the drone together with the circularly polarized WANTENNAX005 antenna by C.A.E.N. RFID (Fig. 6). The reader was fed through the drone battery (P_{TX}=26 dBm). To allow the wireless control, the latter was equipped with the Wi-Fi module Vonets VAP11G-300 according to the procedure suggested by the reader manufacturer. Then, a mobile phone hotspot was exploited to realize the wireless link between the reader and the laptop.

A synchronization between the reader clock and the GNSS acquisition timestamp is necessary for a proper timing management of reader measurements against drone position measurements. For this reason, a trigger event was recorded both in the reader time and in GNSS time.

B. UHF-RFID tags

Fig. 7b shows the grid of 5×5 UHF-RFID tags in a 8 m × 8 m area employed in the outdoor scenario. The inter-tag distance is equal to around 2 m. As shown in the inset of Fig. 7b, from the first to the last row, different tag typologies were used, and their main parameters are in Table III. The use of different tag typologies aims at demonstrating the method effectiveness independently on the tag characteristics. Different tag orientations were also tested, since the reader antenna radiates a circularly polarized field; tags on odd (even) rows are aligned along the x-direction (y-direction), as shown in Fig. 7b.

At the beginning of the experimental campaign, the actual tag positions were geo-referred through the GNSS ground station and the ITALPos network. The geographic coordinates were then transformed into metric (x and y) coordinates with ellipsoidal quote using the Convergo software [39]. Finally, a proper roto-translation was applied to centre the local reference system at the first Alien ALN9640 tag (Fig. 7b). The latter measurements were assumed as the ground truth for the tag position. The same transformation was also applied to the geographic coordinates of the flying drone to get its trajectory in a unified reference system.

As an example, Fig. 8 shows the drone trajectory with almost square-wave path in the local reference system. The antenna path width is around 8 m along both the *x*- and *y*-directions; height variations are less than 1 m and the drone speed varies between 0.1 m/s and 1.3 m/s (Fig. 8b).

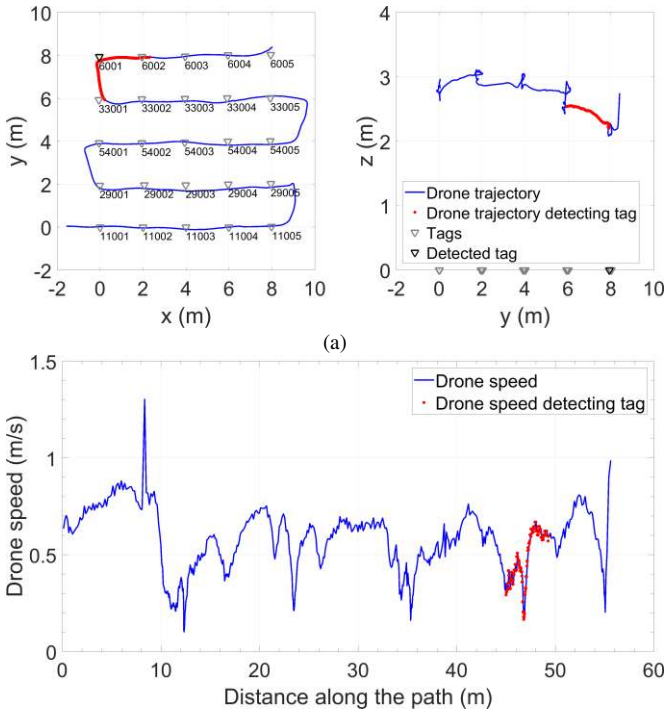

Fig. 8. Example of (a) drone trajectory with almost square-wave path measured with the GNSS receiver and (b) drone speed along the path. Red circle markers represent the trajectory data during the temporal interval in which the tag LABID UH106 #06001 replies to the reader query.

TABLE III
MAIN PARAMETERS OF THE TAGS EMPLOYED IN THE EXPERIMENTAL SETUP.

Tag	*Sizes*	*EPC*	*Chip*	*Chip sensitivity*
Alien ALN9640	8.1 × 94.8 mm^2	#11001-#11005	Alien Higgs-4	-20.5 dBm
Avery Dennison AD-229	8.2 × 95 mm^2	#29001-#29005	MZ-6	-22.1 dBm
Alien ALN9654-G	19 × 93 mm^2	#54001-#54005	Alien Higgs-3	-20 dBm
Smartrac Dogbone	27 × 97 mm^2	#33001-#33005	MZ-4	-19.5 dBm
LABID UH106	8 × 95 mm^2	#06001-#06005	MZ-6	-22.1 dBm

V. EXPERIMENTAL ANALYSIS

The experimental analysis was carried out by processing the RFID measurements for the tags in Fig. 7b. Let us consider the tag #06001 detected from the flying reader antenna along the red path in Fig. 8a. Fig. 9 represents the measured RSSI (circle markers) and phase (square markers) data (f_0=865.7 MHz, ETSI Channel 4). N_r=263 available readings were acquired according to the spatial sampling criteria (11) and along a path 4.33 m long. In such interval, the drone speed varies between 0.17 m/s and 0.67 m/s and the mean value of the reader interrogation repetition time ($\overline{IRT}$) is 36 ms. The total time for tag sample acquisition depends on the drone speed and the trajectory length: in this case it is about 11 s. As the processing time is less than 1 s, it is reasonable assuming that the output rate of the proposed localization method is given by the data acquisition time interval.

An accurate knowledge of the position of the phase centre of the RFID reader antenna [40] represents a critical task, especially when the antenna is close to an electrically large metallic object. At a first approximation, we evaluated the position of the antenna phase centre with an upward shift of 10 cm with respect to the antenna surface, to account for the presence of the drone structure.

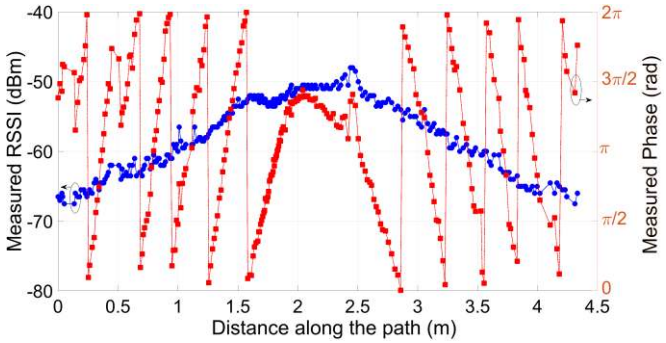

Fig. 9. Measured RSSI (dBm, circular markers) and phase (radians, square markers) with respect to the distance along the path travelled by the drone, when detecting the tag #06001. The actual tag position is [x_{tag}, y_{tag}, z_{tag}]=[-0.04, 7.93, 0] m and other system parameters are as follows: f_0=867.5 MHz, N_r=263, v=[0.17, 0.67] m/s, $\overline{IRT} = 36$ ms .

Fig. 10 shows the 2D matching function (9) obtained by processing measured RSSI and phase values shown in Fig. 9. A well distinct peak appears, confirming the method capability to measure the tag position by employing a drone flying along an arbitrary trajectory with variable speed.

In this case, the peak position is associated to the tag coordinates $\left[x_{tag},\ y_{tag}\right] = \left[0.04, 7.93\right]$ m, while the actual tag position measured with the GNSS system is equal to $\left[x_{tag}, y_{tag}\right] = \left[-0.04, 7.93\right]$ m (tag position ground truth). Thus, the absolute measurement errors are equal to $\varepsilon_x = 8$ cm and $\varepsilon_y < 1$ cm, for the two coordinates, respectively. The measured peak is $C_{peak} = 0.84$ and the measured level of the sidelobe (SL) is 0.69 ($PSLR = 1.21$). The -3 dB measured mainlobe widths are $W_{maj} \times W_{min} = 39$ cm × 18 cm . The widths along the x- and y- directions are $W_x = 19$ cm and $W_y = 28$ cm, for measured synthetic aperture lengths of $D_x = 2.85$ m and $D_y = 2.05$ m .

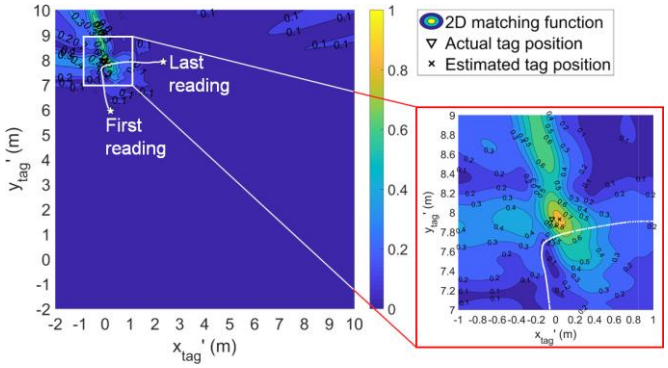

Fig. 10. 2D matching function with respect to the hypothetical tag coordinates in the xy-plane, when processing the measured RSSI and phase samples of tag #06001 as in Fig. 9.

The measurement errors for the x- (circular markers) and y- (square marker) coordinates for the tags in the scenario of Fig. 7b are represented in Fig. 11. In the considered cases, the flying antenna detects each tag along different trajectories with synthetic aperture lengths $\left\{D_x,\ D_y\right\} > 50$ cm . The longer the path run by the flying reader antenna, the lower the measurement error. The mean values and standard deviations are equal to [μ_x, σ_x]=[2.3, 4.2] cm and [μ_y, σ_y]=[-4.4, 5.5] cm, while the maximum measurement errors for the x- and y-coordinates are 8.9 cm and -11.9 cm, respectively. Besides, it is possible to evaluate the measurement error of the distance between the tag and the flying antenna position at the time of the last tag reading, d_{last} . Fig. 12 shows the measurement error $\varepsilon_d = d_{last} - d_{last}$ (triangular marker), and the relative measurement error (star marker) $\varepsilon_{rel-d} = \left(d_{last} - d_{last}\right) \Big/ d_{last}$. The mean value of the distance measurement error is lower than 1 cm.

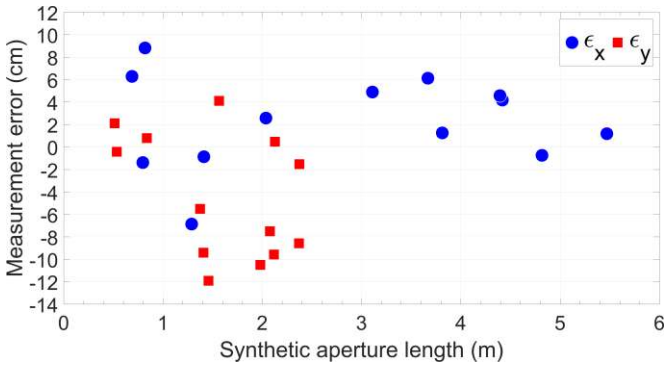

Fig. 11. Measurement errors (cm) for the *x*- (circular markers) and *y*- (square markers) coordinates with respect to the relative synthetic aperture lengths D_x and D_y, for the tags in the outdoor scenario of Fig. 8b.

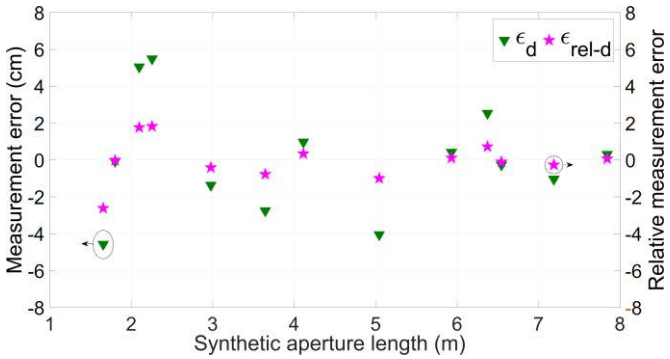

Fig. 12. Measurement error (cm, triangular markers) and relative measurement error (star markers) for the distance between the tag and the flying antenna position at the time of the last tag reading, with respect to the measured synthetic aperture length (D_x+D_y), for the tags in the outdoor scenario of Fig. 7b.

VI. Conclusion

This paper presented a measurement method for positioning of passive tags through a flying UHF-RFID reader and a SAR-based localization processing. The method exploited the knowledge of the reader trajectory given by a differential GNSS system on the drone. By measuring the tag complex backscattered signal along a proper spatial interval, the 2D tag position can be measured even for not rectilinear trajectories of the reader antenna.

A numerical analysis was carried out to evaluate the impact of the possible source of errors in the measurements of the reader trajectory by the GNSS system and of the tag backscattered complex (amplitude and phase) signal.

The experimental analysis was realized in an outdoor scenario by employing commercial RFID hardware and a micro-class unmanned aerial vehicle. Localization errors of centimetre order can be easily achieved without requiring any time-consuming calibration phase. Finally, it is noteworthy that, in real applications, each tag is actually attached to items or pallets; thus, the achieved localization error has to be compared with their size, and localization errors up to a few tens of centimetre can be more than acceptable in many industrial or logistics scenarios.

Acknowledgment

This work was partly funded by Regione Toscana (POR FESR 2014-2020 - Line 1 – R&D Strategic Projects) under project IREAD4.0 (CUP number 7165.24052017.112000028).

The authors want to thank Armando Schiavoni and Claudia Scaramella for their valuable technical support for the deployment of the measurement campaign.

References

[1] P. Daponte, L. De Vito, F. Lamonaca, F. Picariello, S. Rapuano, and M. Riccio, “Measurement science and education in the drone times”, *2017 IEEE International Instrumentation and Measurement Technology Conference (I2MTC)*, Torino, Italy, 2017, pp. 1-6.

[2] P. Daponte, L. De Vito, G. Mazzilli, F. Picariello, and S. Rapuano, “A height measurement uncertainty model for archaeological surveys by aerial photogrammetry”, *Measurement*, vol. 98, pp. 192-198, 2017.

[3] M. Rossi and D. Brunelli, “Autonomous Gas Detection and Mapping With Unmanned Aerial Vehicles”, *IEEE Transactions on Instrumentation and Measurement*, vol. 65, no. 4, pp. 765-775, April 2016.

[4] Ascending Technologies, “UAV application”, 2017. [Online]. Available: http://www.asctec.de/en/uav-uas-drone-applications/.

[5] L. Angrisani, G. D’Alessandro, M. D’Arco, V. Paciello, and A. Pietrosanto, “Autonomous recharge of drones through an induction based power transfer system”, *2015 IEEE International Workshop on Measurements & Networking (M&N)*, Coimbra, Portugal, 2015, pp. 1-6.

[6] Drone Scan, “Stock Take, Physical Inventory, Cycle Counting”, 2017. [Online]. Available: http://www.dronescan.co/info.

[7] The Guardian, “Amazon claims first successful Prime Air drone delivery Amazon”, Dec. 14, 2016. [Online]. Available: https://www.theguardian.com/technology/2016/dec/14/ amazon-claims-first-successful-prime-air-drone-delivery.

[8] S. M. Bae, K. H. Han, C. N. Cha and H. Y. Lee, “Development of Inventory Checking System Based on UAV and RFID in Open Storage Yard”, *2016 International Conference on Information Science and Security (ICISS)*, Pattaya, 2016, pp. 1-2.

[9] J. H. Yang and Y. Chang, “Feasibility study of RFID-Mounted drone application in management of oyster farms”, *2017 IEEE International Geoscience and Remote Sensing Symposium (IGARSS)*, Fort Worth, TX, 2017, pp. 3610-3613.

[10] A. Buffi, P. Nepa,. and R. Cioni, “SARFID on drone: Drone-based UHF-RFID tag localization”, *2017 IEEE International Conference on RFID Technology & Application (RFID-TA)*, Warsaw, 2017, pp. 40-44.

[11] Drones relay RFID signals for inventory control, Massachussets Institute of Technology, August 25, 2017, [Online]. Available: http://news.mit.edu/2017/drones-relay-rfid-signals-inventory-control-0825.

[12] M. Longhi, G. Casati, D. Latini, F. Carbone, F. Del Frate and G. Marrocco, “RFIDrone: Preliminary experiments and electromagnetic models”, *2016 URSI International Symposium on Electromagnetic Theory (EMTS)*, Espoo, 2016, pp. 450-453.

[13] P. Pivato, L. Palopoli. and D. Petri, “Accuracy of RSS-Based Centroid Localization Algorithms in an Indoor Environment”, *IEEE Transactions on Instrumentation and Measurement*, vol. 60, no. 10, pp. 3451-3460, Oct. 2011.

[14] P. Nazemzadeh, F. Moro, D. Fontanelli, D. Macii. and L. Palopoli, “Indoor Positioning of a Robotic Walking Assistant for Large Public Environments”, *IEEE Transactions on Instrumentation and Measurement*, vol. 64, no. 11, pp. 2965-2976, Nov. 2015.

[15] Jae Sung Choi, Byung Rak Son, Hee Kuk Kang, and Dong Ha Lee, “Indoor localization of Unmanned Aerial Vehicle based on passive UHF RFID systems”, *2012 9th International Conference on Ubiquitous Robots and Ambient Intelligence (URAI)*, Daejeon, 2012, pp. 188-189.

[16] G. Greco, C. Lucianaz, S. Bertoldo, and M. Allegretti, “Localization of RFID tags for environmental monitoring using UAV”, *2015 IEEE 1st International Forum on Research and Technologies for Society and Industry Leveraging a better tomorrow (RTSI)*, Turin, 2015, pp. 480-483.

[17] Reshma B. and S. S. Kumar, “Precision aquaculture drone algorithm for delivery in sea cages”, *2016 IEEE International Conference on Engineering and Technology (ICETECH)*, Coimbatore, 2016, pp. 1264-1270.

[18] P. V. Nikitin, R. Martinez, S. Ramamurthy, H. Leland, G. Spiess, and K.V.S. Rao, “Phase Based Spatial Identification of UHF RFID Tags”, *2010 IEEE Int. Conf. RFID*, pp. 102-109, April 2010.

[19] J. Zhou, H. Zhang, and L. Mo, “Two-dimension localization of passive RFID tags using AOA estimation”, *2011 IEEE International Instrumentation and Measurement Technology Conference*, Binjiang, 2011, pp. 1-5.

[20] M. Scherhäufl, M. Pichler, and A. Stelzer, “UHF RFID Localization Based on Phase Evaluation of Passive Tag Arrays”, *IEEE Transactions on Instrumentation and Measurement*, vol. 64, no. 4, pp. 913-922, April 2015.

[21] P. Nepa, F. Lombardini, and A. Buffi, “Method for determining the location of a moving RFID tag”, EP2533173 (A1), IP: University of Pisa, 2011.

[22] A. Buffi, P. Nepa, and F. Lombardini, “A Phase-Based Technique for Localization of UHF-RFID Tags Moving on a Conveyor Belt: Performance Analysis and Test-Case Measurements”, *IEEE Sensors Journal*, vol. 15, no. 1, pp. 387-396, Jan. 2015.

[23] A. Parr, R. Miesen, and M. Vossiek, “Inverse SAR approach for localization of moving RFID tags”, *2013 IEEE International Conference on RFID (RFID)*, Penang, 2013, pp. 104-109.

[24] R. Miesen, F. Kirsch, and M. Vossiek, “UHF RFID Localization Based on Synthetic Apertures”, *IEEE Transactions on Automation Science and Engineering*, vol. 10, no. 3, pp. 807-815, July 2013.

[25] A. Buffi, M. R. Pino, and P. Nepa, “Experimental Validation of a SAR-Based RFID Localization Technique Exploiting an Automated Handling System”, *IEEE Antennas and Wireless Propagation Letters*, vol. 16, pp. 2795-2798, 2017.

[26] Ma Yunfei, Nicholas Selby, and Fadel Adib, “Drone Relays for Battery-Free Networks”, *Proceedings of the Conference of the ACM Special Interest Group on Data Communication (SIGCOMM ‘17)*, pp. 335-347, 2017. (doi: 10.1145/3098822.3098847).

[27] EPC UHF Gen2 Air Interface Protocol Standard. [Online]. Available: https://www.gs1.org/epcrfid/epc-rfid-uhf-air-interface-protocol/2-0-1.

[28] A. Buffi and P. Nepa, “Advanced SARFID: A localization technique for UHF RFID tags”, *2016 URSI International Symposium on Electromagnetic Theory (EMTS)*, Espoo, 2016, pp. 322-325.

[29] CAEN RFID, WANTENNAX019 datasheet, 2017. [Online]. Available: https://caenrfid.com/en/products/wantennax019/

[30] C. E. Shannon, “Communication in the presence of noise”, *Proc. IEEE*, vol. 86, no. 2, pp. 447–457, Feb. 1998.

[31] K. Finkenzeller, *RFID Handbook: Radio-Frequency Identification Fundamentals and Applications*. Hoboken, NJ, USA: Wiley, 2004.

[32] O. Frey, C. Magnard, M. Ruegg and E. Meier, “Focusing of Airborne Synthetic Aperture Radar Data From Highly Nonlinear Flight Tracks”, *IEEE Transactions on Geoscience and Remote Sensing*, vol. 47, no. 6, pp. 1844-1858, June 2009.

[33] Impinj, Low Level User Data Support, 2013. [Online]. Available: https://support.impinj.com/hc/en-us/articles/202755318-Application-Note-Low-Level-User-Data-Support

[34] A. Buffi, A. Michel, P. Nepa, and B. Tellini, “RSSI Measurements for RFID Tag Classification in Smart Storage Systems”, *IEEE Transactions on Instrumentation and Measurement*, vol. 67, no. 4, pp. 894-904.

[35] F. Martinelli, “A Robot Localization System Combining RSSI and Phase Shift in UHF-RFID Signals”, *IEEE Transactions on Control Systems Technology*, vol. 23, no. 5, pp. 1782-1796, Sept. 2015.

[36] IDS, Colibrì IA-3 datasheet, April 2017. [Online]. Available: https://www.idscorporation.com/drones/ids-drones/item/121-ia-3-colibri

[37] TOPCON, Compact Dual Frequency GNSS Board B110, April 2017. [Online]. Available: https://www.topconpositioning.com/sites/default/files/product_files/b110_brochure.pdf

[38] [Online]. Available: http://it.smartnet-eu.com/

[39] [Online]. Available: http://www.centrointerregionale-gis.it/CONVERGO/documenti.asp

[40] A. Kumar, A. D. Sarma, E. Ansari, and K. Yedukondalu, “Improved Phase Center Estimation for GNSS Patch Antenna”, *IEEE Transactions on Antennas and Propagation*, vol. 61, no. 4, pp. 1909-1915, April 2013.